Energy-dispersive measurements of $L\alpha_1$ and Ll x-ray linewidths

Tibor Papp, John L. Campbell, John A. Maxwell, Jian-Xiong Wang, and William J. Teesdale
Guelph-Waterloo Program for Graduate Work in Physics, University of Guelph, Guelph, Ontario, Canada N1G 2W1
(Received 25 April 1991; revised manuscript received 21 August 1991)

Proton-induced L x-ray spectra of heavy elements have been recorded with a Si(Li) x-ray spectrometer of accurately determined resolution function. The intrinsic widths of the Ll and $L\alpha_1$ lines were obtained by a nonlinear-least squares fitting procedure. $L\alpha_1$ widths agree with relativistic independent-particle-model (IPM) calculations, but Ll widths fall some 10–30 % below predictions. This indicates a strong influence of many-body effects on the decay of the $3s$ hole state; a similar influence is already well established for the $2s$ state. Relative intensities of the weak, electric-dipole-forbidden lines Lt and Ls are in good accord with IPM calculations.

PACS number(s): 32.70.Jz, 32.30.Rj

I. INTRODUCTION

It is well established that relativistic independent-particle-model (IPM) calculations are quite successful in predicting the widths of atomic $2p$ hole states but provide values for the widths of $2s$ hole states that are significantly larger than those measured experimentally. Direct measurements [1] of the widths of L_1 x-ray lines in the atomic number region $41 \leq Z \leq 51$ fall well below theory, as do measurements [2] of the Coster-Kronig probabilities f_{12} and f_{13}, which account for a large portion of the width in this region. These observations are reflected in the width compilation of Krause and Oliver [3], and more recent Coster-Kronig data [4] for atoms of higher Z also tend to fall below theory.

The most recent and sophisticated IPM calculations for L subshells are those of Chen, Crasemann, and Mark [5], who calculated relativistic Auger and Coster-Kronig rates from perturbation theory using the Møller operator and Dirac-Hartree-Slater wave functions. Radiative rates were taken from Scofield's calculations [6] using Dirac-Fock wave functions and including exchange and overlap corrections. Except at very high atomic number, the radiative deexcitation is the minor contributor to the width. The discrepancy between measured widths and $2s$ Coster-Kronig probabilities and the frozen-orbital IPM calculation is generally ascribed to the effect of correlations. $2p$ widths and f_{23} Coster-Kronig probabilities exhibit much better, albeit not perfect, agreement with the IPM predictions, indicating that in this case, correlation effects are less important.

It is clearly of interest to examine the situation for 3s hole states, where the predictions of the same frozen-orbital IPM are available [7]. As yet there are no reliable measurements of $3s$ Coster-Kronig probabilities. There are, however, a few measurements of widths of $Ll(L_3M_1)$ x-ray lines [8–11] and for high atomic numbers these depart significantly from theory. Since calculated and measured widths for the L_3 level are in good agreement, this observation indicates that the theory is not successful in predicting M_1 (i.e., $3s$) level widths. The discrepancy between measured and calculated $3s$ widths is some 30–50 % for the atomic number region $69 \leq Z \leq 90$. In contrast to the Ll case, measured widths of $L\alpha_2(L_3M_4)$ and $L\alpha_1(L_3M_5)$ lines [10,12,13] in this atomic number region agree quite well with the IPM predictions. In the region around $Z=50$ measurements of both Ll x-ray linewidths [11] and x-ray photoelectron spectra linewidths [14] give results that are about 10% below the Herman-Skillman IPM treatment of McGuire [15]. Unfortunately, the IPM predictions of Chen, Crasemann, and Mark [7] do not extend below $Z=67$. However, at higher Z the values of Chen, Crasemann, and Mark are rather smaller than those of McGuire; if this difference persists at lower Z, then the measured linewidths would not exhibit major differences from the IPM values of Chen, Crasemann, and Mark.

The paucity of $3s$ width data and the large error bars associated with the few available data points suggest the merit of additional measurements which might help provide a firmer basis for testing theoretical efforts to deal with correlation effects.

II. EXPERIMENT

A. Method

All previous width measurements for L x-ray lines have employed diffraction spectrometers, in the interest of achieving the highest possible resolution. The high degree of collimation that is mandatory lowers the geometric efficiency, and the angle-by-angle mode of data recording lowers the overall volume of data. The Ll line constitutes only $\sim 4\%$ of the overall L_3 x-ray intensity and $<2\%$ of the entire spectrum if all subshells are excited. The result is that the diffraction peak from Ll x-rays is of low intensity and its fitted width has high statistical error.

In this work essentially the opposite approach is adopted. The spectra are recorded with an energy-dispersive Si(Li) x-ray spectrometer, which guarantees high geometric efficiency and simultaneous recording not only of the Ll peak but of the $L\alpha(L_3M_{4,5})$ and other peaks. In this instrument, however, the resolving power is some

ten times worse than that afforded by a crystal spectrometer. The philosophy is that this disadvantage is to a large degree compensated by very large counting statistics and by an accurately determined resolution function. (This philosophy guided our earlier measurements of K x-ray linewidths using germanium spectrometers [16].) It is then important to determine the analytic form of the resolution function and the energy dependence of its parameters over the energy range of interest, 6–15 keV in the present work.

B. Apparatus

The L x-rays were generated by proton-induced ionization in thin film targets, using the Guelph Van de Graaff accelerator. The beam energy was 2.4 MeV for targets in the atomic number range $69 \leq Z \leq 79$ and 3.0 MeV for $Z = 82$ and 90. Targets of 1-50 mg/cm^2 supplied by Micro Matter Inc. included thulium, iridium, lead, and thorium.

The L x-ray spectra were recorded by a Link Series E Si(Li) detector at typical counting rates of under 1000 s^{-1}. This device displayed energy resolution 133 eV [full width at half maximum (FWHM)] at 5.9 keV and 190 eV at 13 keV. A 1-mm-diam tantalum collimator restricted stricted x-rays to the central region of the detector (diameter 6 mm) in which peak distortion by low-energy tailing was both minimum and uniform. This region was established previously by scanning a 0.5-mm-wide pencil of monoenergetic x-rays along diameters and observing the radial dependence of tail-to-peak intensity ratios [17]. A Nuclear Data 575 analog-to-digital converter equipped with an ND595 digital stabilizer recorded the spectra, in which typical Ll and $L\alpha$ peak intensities were 10^6 and 2×10^7, respectively. Figure 1 (upper portion) shows the relevant portion of the L x-ray spectrum of thorium.

In order to determine the response function of the Si(Li) detector, spectra of various monoenergetic x-rays were recorded. These x-rays were provided by a curved-crystal monochromator (radius 25 cm) attached to a microfocus variable-anode x-ray generator such that the target spot was located on the Rowland circle. Targets of elements in the atomic number range $22 \leq Z \leq 47$ provided $K\alpha_1$ lines and in a few cases $K\beta_1$ lines, using diffracting crystals of quartz [(100) and (101)] and lithium fluoride [(200) and (220)]. Exit slits on the Rowland circle directed the diffracted radiation onto a fluorescent screen viewed by a microscope. Once the appropriate x-ray line had been selected by the slits (e.g., the $K\alpha_1$ component of the $K\alpha_{1,2}$ doublet), the screen and microscope were removed and the x-ray beam extracted via an evacuated exit tube with a 0.05-mm Mylar window. The Si(Li) detector was placed in the air just outside this window; the beam entered it via a tantalum collimator as used in the main L x-ray study, and counting rates were adjusted

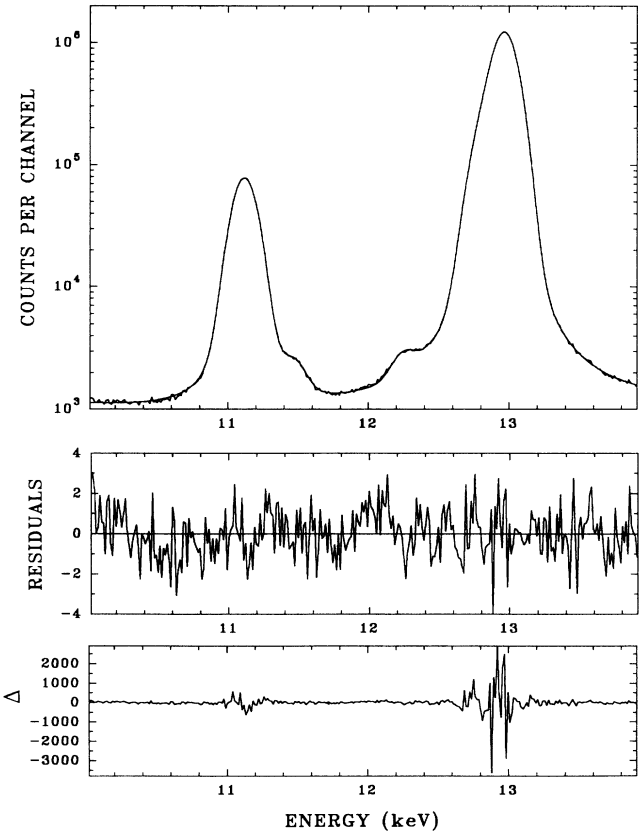

FIG. 1. Details of fit to the region of the thorium L x-ray spectrum containing the electric dipole Ll (11.119 keV) and $L\alpha$ (12.810 and (12.969 keV) lines and the weak electric-dipole-forbidden Lt (11.479 keV) and Ls (12.261 keV) lines. The residues are in units of one standard deviation. △ represents the difference between measured and fitted spectra.

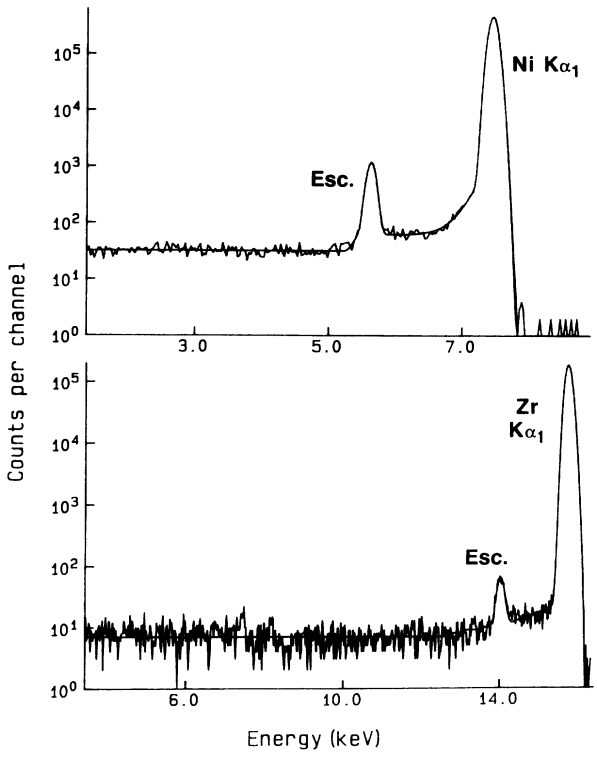

FIG. 2. Fits of Eq. (1) to nickel $K\alpha_1$ and zirconium $K\alpha_1$ lines; the smooth curve is the fit. The K x-rays of the detector's nickel contact, arising from fluorescence, are present in the Zr spectrum.

to be the same as those used in the main study.

Ten replicate measurements were made at each x-ray energy and fitted to a semiempirical resolution function described in Sec. IIC. Figure 2 shows the nickel and zirconium $K\alpha_1$ spectra with the fits superposed as continuous curves.

C. Resolution function

For the detector used here [17] an excellent description of the spectrum is afforded by an analytic line shape in which the degraded events left of the Gaussian full-energy peak are described by an exponential tail $D(i)$, a long flat shelf $S(i)$, extending to zero energy and a truncated flat shelf $S_T(i)$ extending just beyond the silicon escape peak. This function is

$$F(x)=G(x)+D(x)+S(x)+S_T(x)+E(x)\ , \tag{1}$$

where i is a channel number, and

$$G(i)=H_G \exp\left[\frac{-(i-i_0)^2}{2\sigma^2}\right] \tag{2}$$

$$D(i)=\tfrac{1}{2}H_D \exp\left[\frac{i-i_0}{\beta}\right] erfc\left[\frac{i-i_0}{\sigma\sqrt{2}}+\frac{\sigma}{\beta\sqrt{2}}\right] \tag{3}$$

$$S(i)=\tfrac{1}{2}H_S \mathrm{erfc}\left[\frac{i-i_0}{\sigma\sqrt{2}}\right] \tag{4}$$

$$S_T(i)=\tfrac{1}{2}H_{ST}\left[\mathrm{erfc}\left[\frac{i-i_0}{\sigma\sqrt{2}}\right]-\mathrm{erfc}\left[\frac{i-i_T}{\sigma\sqrt{2}}\right]\right], \tag{5}$$

$$G_e(i)=H_e \exp\left[-\frac{(i-i_e)^2}{2\sigma^2}\right]. \tag{6}$$

i_0 is the Gaussian centroid, i_e the escape peak centroid, and i_T the channel where the truncated shelf has fallen to half its height. The H parameters are the heights of the various components and β determines the slope of the exponential tail. The complementary error functions arise from the convolution of simple flat shelf and exponential terms with a unit-area Gaussian to obviate nonphysical sharp edges at $i=i_0$ and $i=i_T$.

The fits of $F(i)$ to the measured spectra were accomplished by a standard nonlinear least-squares method. In each case a weak horizontal background was included. The reduced χ^2 values, normalized to one million counts peak intensity, were typically $\chi_r^2 \simeq 1.9$, indicative of good fits, and the residuals showed only statistical fluctuations. Figure 3 gives the energy dependence of the various parameters of the line-shape function. Since the truncated shelf S_T had very low intensity for x-ray of energy above 12 keV, it was omitted in these cases. As a result there is a discontinuity in the behavior of the exponential tail. By interpolation in the curves of Fig. 3, the parameters corresponding to any desired x-ray energy may be obtained.

D. Analysis of L X-ray spectra

It has been customary in x-ray spectroscopy with Si(Li) detectors to ignore the intrinsic Lorentzian shape of x-ray lines, on the grounds that the Lorentzian width Γ is very much smaller than the detector's resolution (FWHM). However, the effect of the Lorentzian is not restricted to a slight broadening of the spectral peak. It introduces in addition tailing components on the upper and lower edges, which now fall toward zero intensity much more slowly than would a purely Gaussian line shape. On the lower edge this tailing is augmented by the effects of imperfect charge collection, but if due attention is paid to

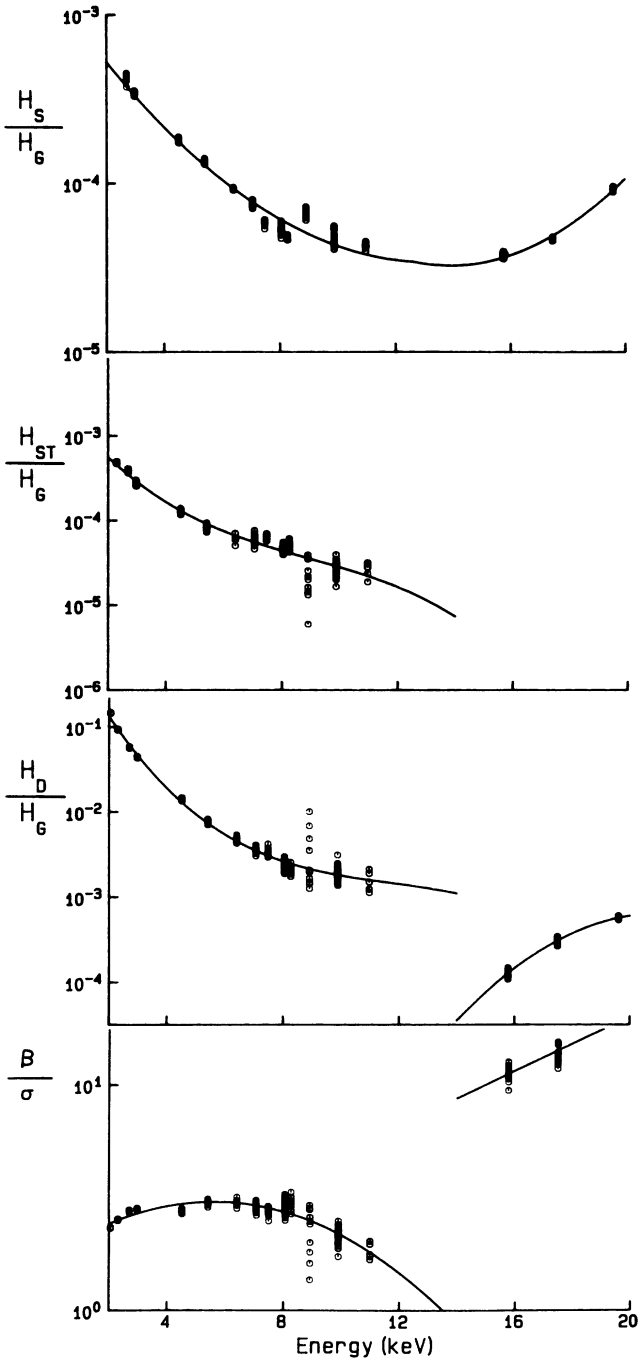

FIG. 3. Energy dependence of the parameters of the Si(Li) detector line shape.

the avoidance of pulse pileup, it is the only source of upper edge tailing. It follows that if well-separated peaks are accumulated to sufficiently high intensities that the tailing is statistically well-defined, and the possibility exists of determining Lorentzian widths by letting their values be variable in a least-squares fit to the spectrum.

The spectral region containing the Ll and $L\alpha$ lines also contains the much less intense $Lt(L_3M_2)$ and $Ls(L_3M_3)$ lines, which are of mixed electric quadrupole and magnetic dipole nature. It can be seen from the measured spectrum in Fig. 1 that the detector resolution is sufficiently good that these lines are clearly discernible and must be included in any function used to model the spectrum. There are therefore five lines to be fitted by the nonlinear-least squares procedure and the model function is

$$F_L(x)=\sum_j F_j(x)\otimes L_j(x) , \tag{7}$$

where $j=l,t,s,\alpha,\eta$,

$F_j(x)$ is given by Eq. (1) and each $F_j(x)$ is convoluted $\otimes$ with the appropriate Lorentzian

$$L(x)=\frac{\Gamma/2\pi}{(x-x_0)^2+(\Gamma/2)^2} . \tag{8}$$

The convolution is effected numerically and in a manner that ensure no loss of peak intensity. In practice only the l,α,η, lines need to be convoluted. In addition a weak lead $L\alpha$ line is present in the spectrum of thorium and was included in the fit. Satellites arising from radiative Auger emission or LM double ionization are of intensity too low to be discernible in fitting these spectra.

The heights of the six lines are variables in the fitting procedure. The overall number of variables is kept to a minimum by adopting the constraints

$$(x_0)_k=A_1+A_2E_k , \tag{9}$$

$$(\sigma_0)_k^2=A_3+A_4E_k . \tag{10}$$

The first of these reflects the linear relationship between energy and the Gaussian centroid of each line. The second reflects the well-known energy dependence of peak width [18]. For this particular detector, it is established from the monoenergetic line shapes that

$$A_4=4.625\times10^{-4}A_2^2 ,$$

and thus only three "calibration" parameters need be determined by the fit, in addition to the six Gaussian heights. The tailing features are matched to the Gaussians using the parametrizations discussed earlier. The background continuum was represented by a quadratic.

The Lorentzian widths $\Gamma(L\alpha_1)$ and $\Gamma(Ll)$, which are in the range 5–25 eV, were variables of the fit, and the ratio $\Gamma(L\alpha_2)/\Gamma(L\alpha_1)$ was assumed to be the theoretically calculated value of Ref. [6]. Departures of a few percent from this assumed value of the ratio were found to have no significant influence on the quality of the fit or on the results derived from it. It was observed that omission of the Lorentzian convolution resulted in Lt and Ls intensities twice as large as those obtained in the main fit; this emphasizes the importance of a proper inclusion of the natural line shape.

Finally target thickness corrections were made to the $I(Ll)/I(Lt)$ and $I(Ll)/I(Ls)$ by numerical integration of the x-ray yield, using appropriate values of proton stopping powers and x-ray attenuation coefficients [19]. The correction ranged from 10% to 20% across the range of target elements.

TABLE I. Measured x-ray intensity ratios involving the electric-dipole-forbidden lines Lt and Ls.

Z	$\frac{I(Ll)}{I(Lt)}$ Measured	Calc. (20)	$\frac{I(Ll)}{I(Ls)}$ Measured	Calc. (20)
69	115±42	117.3	147±40	106.9
77	102±20	102	128±38	92.3
82	93±14	95.3	113±20	86.2
90	80±7	88	106±13	80.0

III. RESULTS AND DISCUSSION

Details of a fit in the case of the thorium L x-ray spectrum are presented in Fig. 1. The reduced χ^2 value of 1.9 per million counts is typical of the entire set of spectra.

While the residues and the χ^2 values provide two means of assessing goodness of fit, the relative intensities of the various x-ray lines present another criterion. It is reasonable to expect good agreement between the observed values of the $I(Ll)/I(Lt)$ and $I(Ll)/I(Ls)$ intensity ratios and the Dirac-Hartree-Slater predictions of Scofield [20]. [While there are only two measurements [21,22] known to us of the ratios involving the weak electric-dipole-forbidden lines, the available wavelength-dispersive data for $I(L\alpha_2)/I(L\alpha_1)$ do agree well with theory.] Table I and Fig. 4 provide the comparison. The

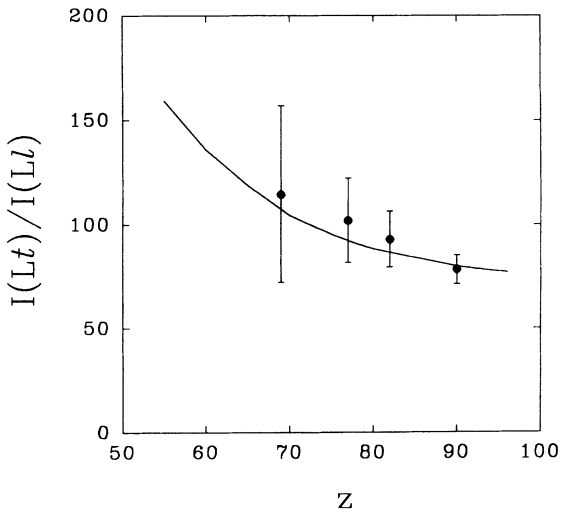

FIG. 4. Comparison of measured (solid circles) and theoretical values (curve) of the intensity ratios of the Ll and Lt lines.

TABLE II. Lorentzian widths of Ll and $L\alpha_1$ x-ray lines.

Z	$\Gamma(Ll)$ Measured	Calc. (7)	$\Gamma(L\alpha_1)$ Measured	Calc. (7)
69	16.8±2.1	20.55	5.5±1.5	5.64
77	18.0±0.9	23.1	8.2±0.2	7.66
82	21.6±0.2	24.65	9.5±0.2	8.74
90	25.1±0.1	27.06	12.1±0.1	11.77

good agreement of measured and predicted x-ray intensity ratios may be regarded either as a useful test of the theory or as confirmation that the quality of fit is good. We prefer the latter since it provides support for the Γ values provided by the fit.

The measured Γ values are compared with IPM predictions and with previous measurements in Table II and Figs. 5 and 6. The IPM values represent the sums of the L_3 and M_5 level widths in the $L\alpha_1$ case and the L_3 and M_1 level widths in the Ll case. In an attempt to estimate the errors in these Γ values the least-squares fits were repeated with the intrinsic detector tailing ignored, i.e., all the tailing attributed to the Lorentzian effects; this resulted in an increased Γ value; the entire error estimate was then obtained by reflecting this shift in the opposite direction. This is obviously a very conservative error estimate, but one that we feel is useful in that it tends to

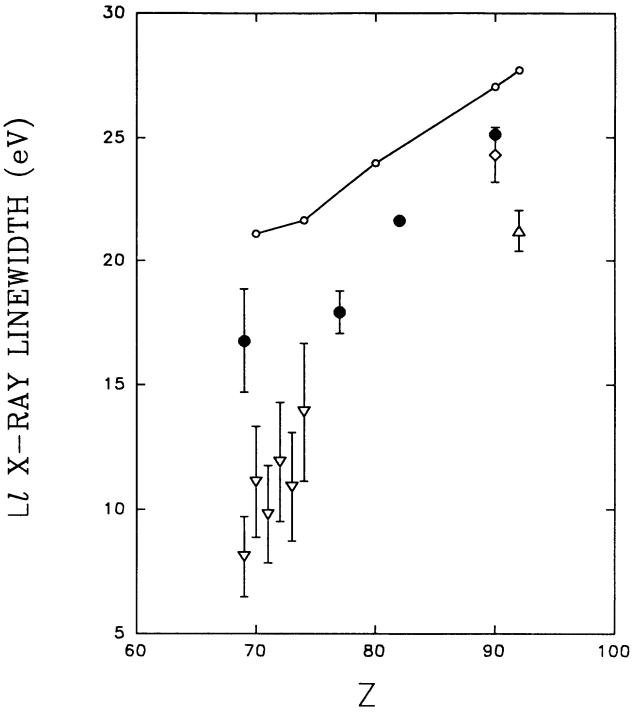

FIG. 6. Lorentzian width of the Ll x-ray line. The lines joining open circles represent the IPM predictions. Sources of the data points are as follows: ●, present data; ▽, Salem and Lee [8]; △, Merrill and DuMond [9]; ◇, Amorim *et al.* [13].

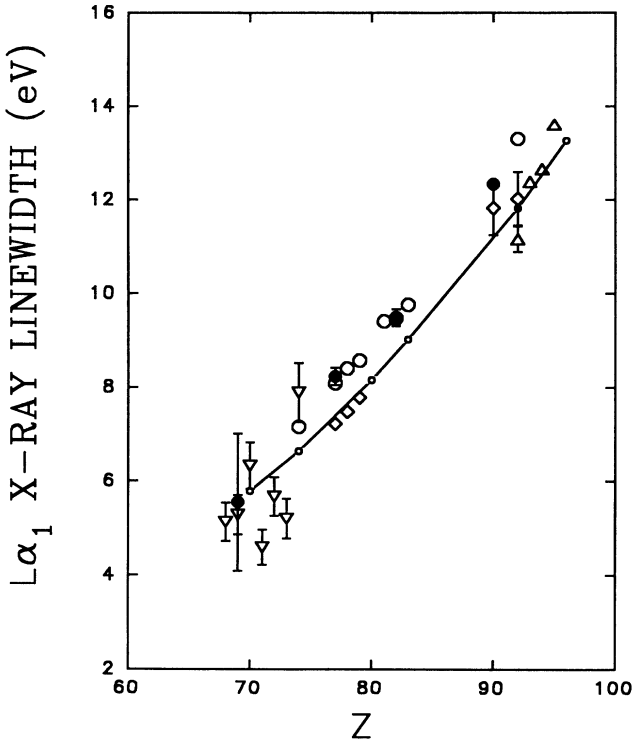

FIG. 5. Lorentzian width of the $L\alpha_1$ x-ray line. The lines joining open circles represent the IPM predictions. Sources of the data points are as follows: ●, present data; ▽, Salem and Lee [8]; △, Merrill and DuMond [9]; ○, Williams [12]; ◇, Amorim *et al.* [10,13].

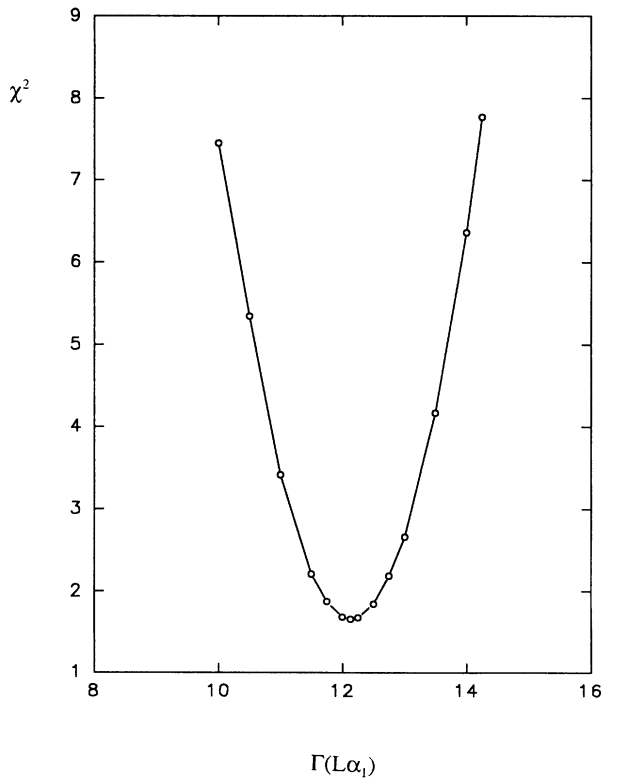

FIG. 7. Dependence of goodness of fit to L x-ray spectrum upon assumed Lorentzian width of the $L\alpha_1$ line.

suggest that the previous set of Ll widths may be erroneously low in value. (The same conservative approach was taken in estimating error in the intensity ratios.) For high-Z values there is little intrinsic tailing and the results are rather accurate. An idea of the rather strong sensitivity of χ_r^2 to the Γ value is obtained from Fig. 7, where we plot χ_r^2 vs $\Gamma(L\alpha)$ as $\Gamma(L\alpha)$ is set at a series of fixed values for the case of thorium.

IV. CONCLUSIONS

Overall, measured Lorentzian widths for the $L\alpha_1$ line in the atomic number region $69 \leq Z \leq 90$ are in fairly good agreement with the relativistic IPM predictions of Chen, Crasemann, and Mark [7]. The significant scatter within the measured data sets of Salem and Lee [8] in the $Z=70$ region and of Merrill and DuMond [9] in the $Z=90$ region may indicate that associated errors are somewhat larger than were estimated by these authors. The data of Williams [12] lie very slightly above the theoretical values. It is interesting that our data show the same trend, but any discrepancy is not a large one.

Ll linewidths measured in this work and in previous crystal spectrometer work fall significantly below theoretical IPM predictions. The discrepancy is considerably less for the present data, which may be somewhat more accurate given our treatment of the resolution function, and for the thorium datum of Ref. [10]. Since L_3 level widths are in good agreement with theory the discrepancy with theory must be attributed to a serious overestimate of the M_1 ($3s$) level width by the independent-particle model.

The $3s$ level thus displays the same striking disparity from independent-particle-model predictions as does the $2s$ level. There is a need for a many-electron treatment of these level widths along the lines of that performed [23] for N-shell linewidths.

ACKNOWLEDGMENT

This work was supported by the Natural Sciences and Engineering Research Council of Canada through award of an operating grant to J.L.C. and support of T.P.

[1] P. Putila-Mäntylä, M. Ohno, and G. Graeffe, J. Phys. B **17**, 1735 (1984).
[2] S. L. Sorenson, R. Carr, S. J. Schaphorst, S. B. Whitfield, and B. Crasemann, Phys. Rev. A **39**, 6241 (1989).
[3] M. O. Krause and J. H. Oliver, J. Phys. Chem. Ref. Data **8**, 328 (1979).
[4] U. Werner and W. Jitschin, Phys. Rev. A **38**, 4009 (1988).
[5] M. H. Chen, B. Crasemann, and H. Mark, Phys. Rev. A **24**, 177 (1981).
[6] J. H. Scofield, Phys. Rev. A **10**, 1507 (1974).
[7] M. H. Chen, B. Crasemann, and H. Mark, Phys. Rev. A **21**, 449, (1980); **27**, 2989 (1983).
[8] S. I. Salem and P. L. Lee, Phys. Rev. A **10**, 2033 (1974).
[9] J. Merrill and J. W. M. DuMond, Ann. Phys. (N.Y.) **14**, 166 (1961).
[10] P. Amorim, L. Salguerio, F. Parente, and J. G. Ferreira, J. Phys. B **21**, 3851 (1988).
[11] M. Ohno, P. Putila-Mäntylä, and G. Graeffe, J. Phys. B **17**, 1747 (1984).
[12] J. H. Williams, Phys. Rev. **45**, 71 (1934).
[13] P. Amorim, L. Salgueiro, F. Parente, and J. E. Ferreira, Nucl. Instrum. Methods A **255**, 56 (1987).
[14] J. C. Fuggle and S. F. Alvarado, Phys. Rev. A **22**, 1615 (1980).
[15] E. J. McGuire, Phys. Rev. A **5**, 1043 (1972).
[16] J. L. Campbell, P. L. McGhee, J. A. Maxwell, R. W. Ollerhead, and B. Whittaker, Phys. Rev. A **33**, 986 (1986).
[17] J. L. Campbell and J.-X. Wang, X-Ray Spectrom. **20**, 191 (1991).
[18] G. F. Knoll, Radiation Detection and Measurements, 2nd ed. (Wiley, New York, 1989), p. 455
[19] J. A. Maxwell, J. L. Campell, and W. J. Teesdale, Nucl. Instum. Methods B **43**, 218 (1989).
[20] J. H. Scofield, Lawerence Livermore Laboratory Report No. UCRL-51231, 1972 (unpublished).
[21] H. Maria, J. Dalmasso, G. Ardission, and A. Hachem, X-Ray Spectrom. **11**, 79 (1982).
[22] D. D. Cohen, Nucl. Instrum. Methods A **267**, 492 (1988).
[23] M. Ohno and G. Wendin, Phys. Rev. A **31**, 2318 (1985).